Check for updates

Geophysical Research Letters

RESEARCH LETTER
10.1029/2026GL124581

Sandy Turbidity Current Acts as a Rusty Carbon Pump at the Shelf Edge

Zhuoyue Zhang[1], Chenglong Wang[1], Tianyu Chen[2], Rui Bao[3], Zicheng Chen[1], Xiao Huang[1], Yang Zhang[4], and Xinqing Zou[1,5]

[1]School of Geography and Ocean, Science Ministry of Education Key Laboratory for Coast and Island Development, Nanjing University, Nanjing, China, [2]State Key Laboratory of Critical Earth Material Cycling and Mineral Deposits, School of Earth Sciences and Engineering, Nanjing University, Nanjing, China, [3]Frontiers Science Center for Deep Ocean Multispheres and Earth System, and Key Laboratory of Marine Chemistry Theory and Technology, Ministry of Education, Ocean University of China, Qingdao, China, [4]School of History Culture and Tourism, Fuyang Normal University, Fuyang, China, [5]Collaborative Innovation Center of South China Sea Studies, Nanjing University, Nanjing, China

Abstract Sandy turbidity currents (STCs) efficiently sequester organic carbon (OC) through rapid burial. Yet our understanding of OC preservation within STC deposits remains far less constrained, especially considering STC deposits as an inferred major sink for iron-bound OC (Fe-OC), a long-term stabilized form of OC. Here, we investigate a sediment core with five STC events from the northern slope of the South China Sea (SCS) and compare our observations against a globally compiled sedimentary Fe-OC data set synthesized from published literature. We demonstrate that STC deposits host a higher Fe-OC contribution (22.1% ± 7.6%) than background deposits. STCs drive rapid Fe-OC transportation from shelf to slope under elevated accumulation rates (185.4 ± 84.6 g m^{-2} $time^{-1}$). This process shields Fe-OC from remineralization and favors the formation of refractory OC stabilized within iron matrices. We propose that STCs constitute a "rusty carbon pump," and that continental slopes represent potential hotspots for long-term Fe-OC preservation.

Plain Language Summary Sandy turbidity currents are fast-moving and sandy sediment-laden underwater flows that cascade down continental slopes. They are widely recognized as an efficient natural pathway for oceanic organic carbon sequestration via rapid sediment burial. Yet the mechanisms governing organic carbon (OC) preservation within these geological processes remain incompletely understood, especially regarding their capacity to store stable iron-bound OC (Fe-OC). Here, we investigate a sediment core with five turbidite events from the northern slope of the South China Sea and compare our Fe-OC observations against global sedimentary carbon sink data sets. Our analyses reveal that sandy turbidity current (STC) deposits host a substantially higher fraction of Fe-OC (22.1% ± 7.6%) than background deposits within the core. Turbidity current events rapidly transport Fe-OC from shallow continental shelves to deep slope settings, supporting elevated carbon accumulation rates of 185.4 ± 84.6 g m^{-2} $time^{-1}$. Such rapid transport and burial shields Fe-OC from degradation prevalent under typical background sedimentation and facilitates the preservation of refractory carbon bound to iron minerals. Collectively, our findings confirm that STCs act as an effective "rusty carbon pump," and continental slope settings constitute critical hotspots for long-term OC preservation.

Key Points:

- Sandy turbidity current (STC) acts as a rapid accumulation pump for iron-bound organic carbon (OC)
- Reactive iron within STC deposits preferentially captures and preserves refractory iron-bound OC
- Continental slopes act as hotspot regions and potential long-term sinks for iron-bound OC

Supporting Information:

Supporting Information may be found in the online version of this article.

Correspondence to:

C. Wang and X. Zou,
clwang@nju.edu.cn;
zouxq@nju.edu.cn

Citation:

Zhang, Z., Wang, C., Chen, T., Bao, R., Chen, Z., Huang, X., et al. (2026). Sandy turbidity current acts as a rusty carbon pump at the shelf edge. *Geophysical Research Letters*, *53*, e2026GL124581. https://doi.org/10.1029/2026GL124581

Received 25 MAY 2026
Accepted 18 SEP 2026

Author Contributions:

Conceptualization: Zhuoyue Zhang, Chenglong Wang, Tianyu Chen, Rui Bao, Zicheng Chen, Xiao Huang, Yang Zhang, Xinqing Zou
Data curation: Zhuoyue Zhang, Chenglong Wang, Xiao Huang, Yang Zhang, Xinqing Zou
Formal analysis: Zhuoyue Zhang, Chenglong Wang, Zicheng Chen, Xiao Huang, Yang Zhang, Xinqing Zou
Funding acquisition: Zhuoyue Zhang, Chenglong Wang, Tianyu Chen, Rui Bao, Zicheng Chen, Xiao Huang, Yang Zhang, Xinqing Zou

© 2026 The Author(s). Geophysical Research Letters published by Wiley Periodicals LLC on behalf of American Geophysical Union.
This is an open access article under the terms of the Creative Commons Attribution-NonCommercial-NoDerivs License, which permits use and distribution in any medium, provided the original work is properly cited, the use is non-commercial and no modifications or adaptations are made.

1. Introduction

Organic carbon (OC) burial in marine sediment represents a primary long-term sink for atmospheric CO_2, sequestering carbon within the geosphere over geological timescales (Berner, 1982; Hedges et al., 1997). River deltas and continental shelves serve as key hotspots of OC burial (Bianchi et al., 2018), accounting for up to 80% of OC burial in modern oceans (Burdige, 2007). However, advancing insights into OC burial dynamics within turbidites formed by turbidity current processes have challenged this longstanding paradigm. Turbidity currents drive rapid sediment accumulation (e.g., 0.5–20.0 cm/year; Dennielou et al., 2017), facilitating efficient burial of coarse plant debris associated with sandy turbidity current (STC) deposits in marine sediments (Hage et al., 2020; Lee et al., 2019). The extraordinary OC burial efficiency of STC deposits marks them as a newly recognized carbon sink hotspot (Galy et al., 2007; Kao et al., 2014), indicating that global estimates of marine sediment OC burial require reassessment due to substantial enhancement of OC burial flux mediated by STCs (Galy et al., 2007; Talling et al., 2024).

Investigation: Zhuoyue Zhang, Chenglong Wang, Zicheng Chen, Xiao Huang, Yang Zhang, Xinqing Zou
Methodology: Zhuoyue Zhang, Chenglong Wang, Tianyu Chen, Rui Bao, Zicheng Chen, Xiao Huang, Yang Zhang, Xinqing Zou
Software: Zhuoyue Zhang, Chenglong Wang, Yang Zhang, Xinqing Zou
Supervision: Zhuoyue Zhang, Chenglong Wang, Tianyu Chen, Rui Bao, Zicheng Chen, Xiao Huang, Yang Zhang, Xinqing Zou
Writing – original draft: Zhuoyue Zhang, Chenglong Wang
Writing – review & editing: Zhuoyue Zhang, Chenglong Wang, Tianyu Chen, Rui Bao, Zicheng Chen, Xiao Huang, Yang Zhang, Xinqing Zou

The carbon sequestration capacity of STC deposits in estuaries or fjords is predominantly reflected in the substantial enhancement of terrestrial OC sequestration, such as biospheric OC derived from vegetation and soil (Galy et al., 2015; Hage et al., 2020, 2022). Furthermore, numerous STCs occurring offshore, particularly on continental slopes adjacent to broad continental shelves (Nittrouer et al., 2021; Talling et al., 2024), demonstrate a distinct carbon sequestration capacity. Existing research has traditionally held that STCs played a minor role in the transport and burial of OC in the shelf-edge canyons (Amaro et al., 2016; Talling et al., 2024). However, STCs might influence the interaction between reactive iron (Fe_R) and OC, and provide unique forming conditions for the iron-bound OC (Fe-OC) sink, that is, the "rusty carbon sink" (Lalonde et al., 2012; Miao et al., 2023). Fe_R exhibits strong adsorption and coprecipitation capacities, forming stable, recalcitrant Fe-OC complexes (L. Hu et al., 2023). This interaction markedly decreases OC degradation induced by physical perturbation and microbial remineralization, thereby allowing long-term geological preservation of OC (Chen et al., 2024; Faust et al., 2021).

Efficient sediment transport and shifts in sediment deposition locations serve as potential controls on the Fe-OC sequestration capacity of STC. First, the Fe-OC burial flux on the continental shelf (14.6 ± 5.7 Tg C yr^{-1}) accounts for approximately 20% of the total OC (TOC) (Zhao et al., 2018), making it an important Fe-OC provider on the continental slope. Second, large quantities of coarse-grained material are transported from the continental shelf by STCs (Gao et al., 2019; Li et al., 2017), forming sandy aerobic environments that favor the association of Fe_R and OC, which probably render the continental slope a potential hotspot for the formation and burial of Fe-OC (Z. Zhang, Lu, et al., 2024; Z. Zhang, Zhang, et al., 2024; Zhao et al., 2018). The coarse-grained, high-porosity and permeability STC deposits during the burial process mainly sustain high oxygen availability, facilitating redox interface migration and triggering the formation of iron oxides and the adsorption of OC (Burdige & Komada, 2025; Zhou et al., 2024). Emerging evidence reveals that enrichment of redox-sensitive metals—including uranium and molybdenum—within the sandy sediments of this setting exhibits a robust link with Fe_R distributions (Jokinen et al., 2020; Tribovillard et al., 2006). This connection highlights that the rusty carbon sink in STC deposits may play a pivotal role in the deep-marine sedimentary carbon cycle. In general, the STCs are capable of transporting sediments directly from the continental shelf to the slope and even the deep ocean (Talling et al., 2024), creating conditions conducive to the formation, rapid burial, and efficient preservation of redox-sensitive yet physically recalcitrant Fe-OC. Therefore, STC might function as a previously unappreciated, rapid cross-sphere Fe-OC pump across continental margins to regulate the mechanisms underlying iron-carbon coupling.

Current academic understanding of Fe-OC formation and sink capacity focuses on shallow-water depositional settings, such as estuaries and continental shelves (Shields et al., 2016; Zhao et al., 2023). Within sediment accumulation via such steady depositional processes, the preservation of Fe-OC is collectively constrained by sedimentary environment, Fe_R constituents, and OC sources (Chen & Wang, 2026; L. Hu et al., 2023; Zhao et al., 2023). Nevertheless, the preservation patterns of Fe-OC within high-energy sedimentary processes represented by STC are yet to be fully elucidated. Critical gaps remain regarding the historical record of Fe-OC in STC deposits and the roles of rapid STC processes in driving Fe-OC accumulation and global CO_2 sequestration. Therefore, current scientific questions remain regarding the contribution and characteristics of Fe-OC within STC deposits, and the impact of STC on the accumulation and preservation of Fe-OC.

Here, we analyzed a 267 cm-long sediment core (Q11) with STC records from the Shenhu area on the northern continental slope of the South China Sea (SCS) (Figure 1). Furthermore, we also analyzed 10 surface sediment samples and collected 65 literature data from Lin et al. (2024) for comparative analysis (Figure 1a; Table S3 in Supporting Information S1). First, we conducted sedimentological and geochemical analyses to identify STC activities and associated carbon responses. Second, we quantified the Fe_R and Fe-OC contents and performed thermogravimetric analysis (TGA) to constrain the geochemical characteristics of Fe-OC in STC deposits. Finally, we evaluated the OC and Fe-OC accumulation rates in the STC deposit to explore its global implications for the "rusty carbon sink."

2. Materials and Methods

2.1. Study Area and Sampling

The study area is situated within the Pearl River Mouth Basin and is part of the Baiyun sag, which is located between the Shenhu canyon system and the Dongsha uplift (Figure 1a). This area has been susceptible to frequent

19448007, 2026, 20, Downloaded from https://agupubs.onlinelibrary.wiley.com/doi/10.1029/2026GL124581, Wiley Online Library on [18/10/2026]. See the Terms and Conditions (https://onlinelibrary.wiley.com/terms-and-conditions) on Wiley Online Library for rules of use; OA articles are governed by the applicable Creative Commons License

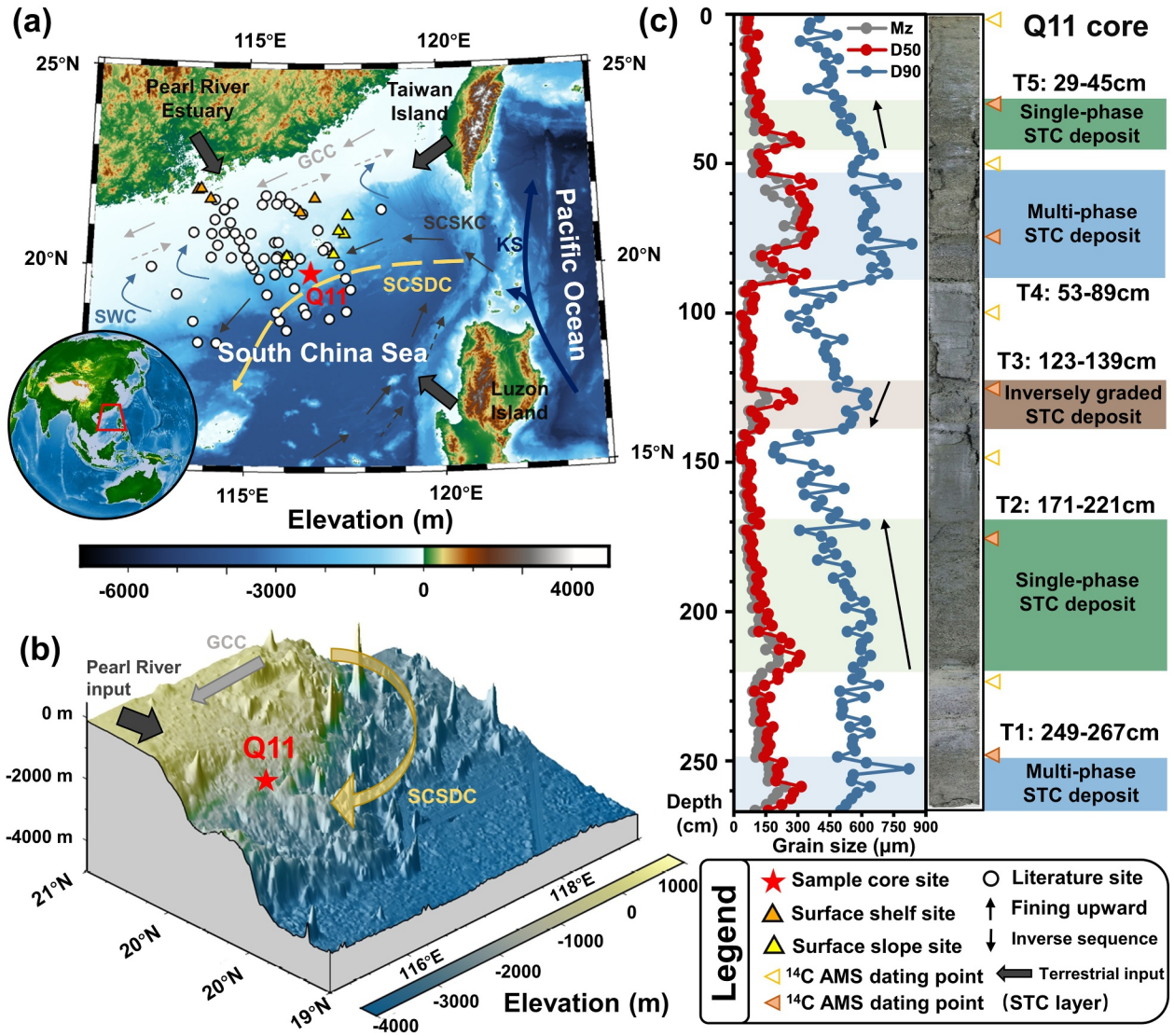

Figure 1. Regional setting and detailed sedimentary log of core Q11 on the northern South China Sea (SCS) slope. (a) Map showing sampling location and major regional ocean currents; Arrows are major oceanic currents redrawn from Lin et al. (2024), including the Guangdong coastal current, SCS warm current (SWC), SCS branch of the Kuroshio current (SCSKC), South China Sea deep-water current, and Kuroshio current. (b) The topography and landform features in the sampling area. (c) High-resolution core scan images of core Q11 paired with the continuous grain-size profile, clearly distinguishing hemipelagic mud intervals and five sandy turbidite units (T1–T5) bounded by basal scour surfaces.

turbidity currents since the last glacial period (Bernhardt & Schwanghart, 2025; Y. Zhang et al., 2018), providing an ideal natural laboratory to investigate STC events and event-related Fe-OC characteristics and accumulation.

The field investigation was conducted on board the research vessel "Xiangyanghong 18" from August to September 2020. A gravity core Q11 (116°38.3′E, 19°54.2′N) was collected from the northern continental slope region of the SCS at a water depth of 1,311 m (Figures 1a and 1c). The core site sits off the main canyon axis and on a canyon levee, an ideal setting to capture STC events. The core Q11 has a recovered length of 267.0 cm, which is bathed in SCS Intermediate Water. The core Q11 is dominated by alternating hemipelagic deposits and episodically abundant foraminiferal-sandy turbidites. In addition, one cruise was completed in the northern SCS onboard the R/V Shiyan 1 in October 2019. We collected 10 surficial sediment samples (0–5 cm) from the northern shelf and slope of the SCS using a box corer (Figure 1a). All sediment samples were stored at −20°C and then freeze-dried before laboratory analysis.

19448007, 2026, 20, Downloaded from https://agupubs.onlinelibrary.wiley.com/doi/10.1029/2026GL124581, Wiley Online Library on [18/10/2026]. See the Terms and Conditions (https://onlinelibrary.wiley.com/terms-and-conditions) on Wiley Online Library for rules of use; OA articles are governed by the applicable Creative Commons License

19448007, 2026, 20, Downloaded from https://agupubs.onlinelibrary.wiley.com/doi/10.1029/2026GL124581, Wiley Online Library on [18/10/2026]. See the Terms and Conditions (https://onlinelibrary.wiley.com/terms-and-conditions) on Wiley Online Library for rules of use; OA articles are governed by the applicable Creative Commons License

2.2. Sedimentological Analysis of Samples

To constrain the core Q11 chronology and accurately distinguish turbidite intervals, we conducted radiocarbon dating, grain size, mineralogy, and elemental composition analyses. Five planktonic foraminifera samples with no turbidite and another five samples with turbidite were taken from core Q11 for radiocarbon dating. Grain size was analyzed using a laser diffraction particle size analyzer (Mastersizer 2000). Specific surface area (SSA) was determined by nitrogen adsorption on an automatic surface area analyzer (BSD-PS4). Non-destructive, continuous core scanning for elemental concentrations was performed on the Cox System Itrax Core Scanner, equipped with a chromium tube as the X-ray source. X-ray diffraction measurements were performed on a Bruker AXS D8 Theta-Theta diffractometer with a SolX detector using Co Kα radiation. More details are shown in Text S1–S4 in Supporting Information S1. In addition, the mean grain size (Mz) of 10 surficial samples originates from Z. Zhang et al. (2025).

2.3. Geochemical Analysis of Samples

To characterize the total OC (TOC) and Fe-OC in the core Q11, we adopted the bicarbonate-citrate buffered dithionite reduction (DCB) method established by Lalonde et al. (2012) to separate and quantify Fe_R and Fe-OC contents. TOC, total nitrogen contents, and stable carbon isotope ($\delta^{13}C$) of the bulk samples, post-DCB samples, and control samples were analyzed using the Thermo Flash 2000 Elemental Analyzer interfaced to a MAT-253 isotope ratio mass spectrometer. The Fe_R collected in the supernatant of the post-DCB samples was quantified by ICP-OES (iCAP6300). More details are shown in Text S5 in Supporting Information S1. To explore the degradation resistance and thermal stability of TOC and Fe-OC, the thermogravimetric analysis (TGA) of the bulk samples and post-DCB samples was performed using a PerkinElmer TGA8000. More details are provided in Text S6 in Supporting Information S1. In addition, the Fe_R and Fe-OC of 10 surficial samples originate from Z. Zhang et al. (2025), and the $\delta^{13}C$ of post-DCB samples and control samples were acquired following the aforementioned method.

2.4. Data Integration and Analysis

To elucidate the sedimentary environments and OC characteristics of the northern SCS shelf and slope, we compiled the Mz and OC data set of surface sediment samples from previous studies. To enable a comparative assessment of $f_{Fe\text{-}OC}$ and Fe-OC accumulation rates across global sedimentary carbon sinks, we compiled Fe-OC and $f_{Fe\text{-}OC}$ data from diverse depositional environments worldwide, including coastal wetlands, estuarine deltas, continental shelves, deep-sea and slope settings, fjords, and trenches. In addition, we compiled dry bulk density and sedimentation rate (or direct mass accumulation rate) data from the corresponding sites of the Fe-OC records. More details are shown in Text S7 in Supporting Information S1.

Analysis of the significance of the differences in the variables was performed using SPSS (SPSS 26.0). The Shapiro-Wilk test was applied to assess the normality of response variables. As most variables exhibited non-normal distributions, the Kruskal–Wallis ANOVA test was selected to assess statistical variability in different layers, followed by Dunn's test for post hoc multiple comparisons. Spearman correlations were performed between OC properties and sedimentary characteristics from each layer using Origin software (version 2023). All statistical analyses were performed with a significance level of 0.05.

3. Results and Discussions

3.1. Sedimentary Records of STC and Carbon Response

Substantial variability of bulk grain size properties in Core Q11 displays that frequent turbidites at various scales have extensively disrupted the hemipelagic depositional sequence (Figure 2g; Figure S1 in Supporting Information S1). There are five layers (T1–T5) that exhibit distinct turbidite characteristics identified in Core Q11 (Figure 1c; Figure S2 in Supporting Information S1). For each STC event in Core Q11, three diagnostic signatures of STC have been identified in sedimentary records: (a) Sand constitutes the dominant sedimentary component (72.4% ± 10.1%, Figure 2f); (b) the upward-fining grain-size sequence and underlying scour structure (Figures S1 and S3 in Supporting Information S1); (c) discontinuity in elemental and mineralogical compositions (Figures S4 and S5 in Supporting Information S1).

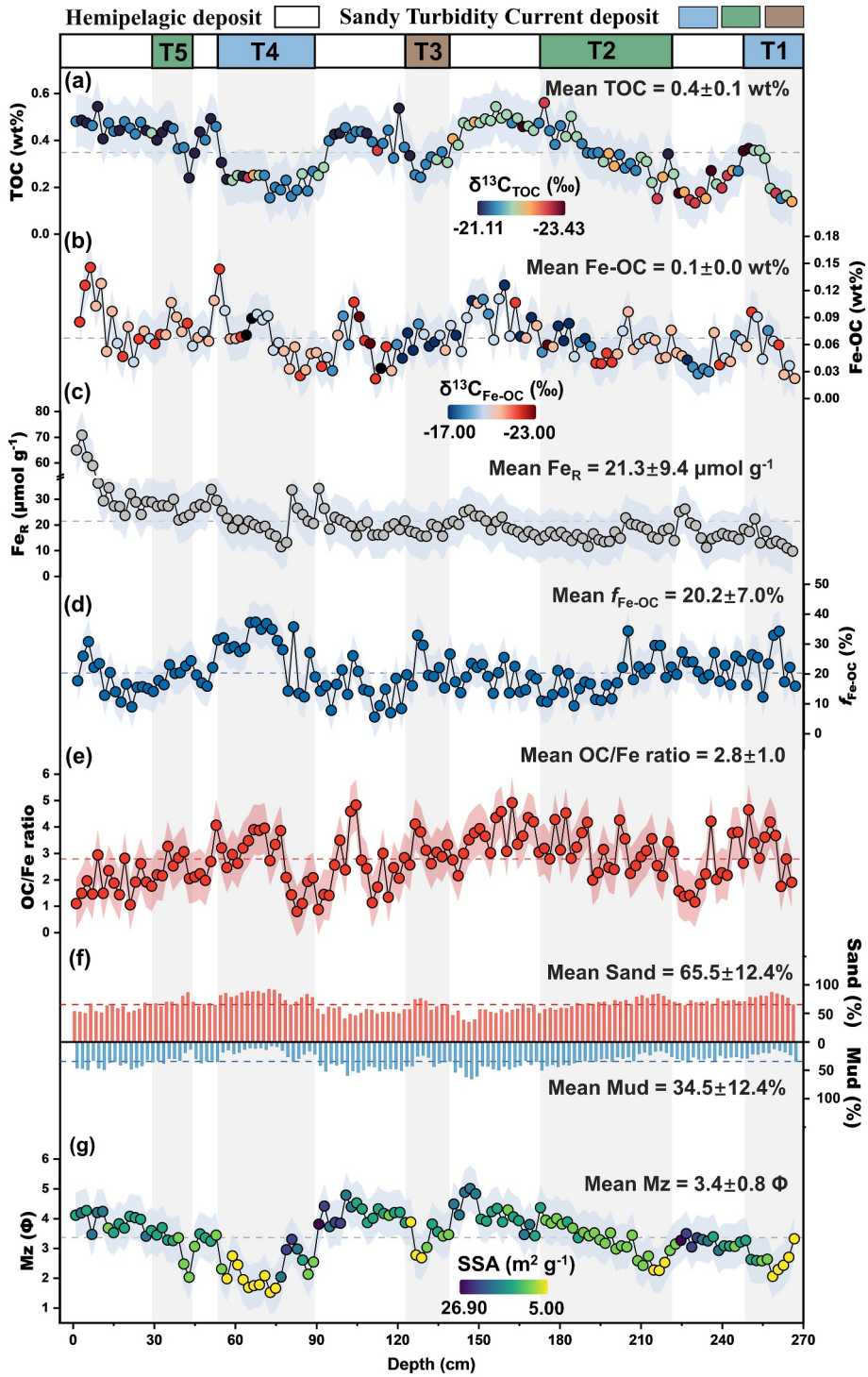

Figure 2. The record of sedimentary and geochemical properties in core Q11 on the northern slope of the South China Sea; (a) The total organic carbon (TOC) content and $\delta^{13}C_{TOC}$ value; (b) The Fe-OC content and $\delta^{13}C_{Fe\text{-}OC}$ value; (c) The Fe_R content; (d) The proportion of Fe-OC to TOC ($f_{Fe\text{-}OC}$); (e) The organic carbon/Fe ratio; (f) The sediment texture proportion; (g) The mean grain size (Mz) and specific surface area value. The gray background represents the sandy turbidity current event layer.

19448007, 2026, 20, Downloaded from https://agupubs.onlinelibrary.wiley.com/doi/10.1029/2026GL124581, Wiley Online Library on [18/10/2026]. See the Terms and Conditions (https://onlinelibrary.wiley.com/terms-and-conditions) on Wiley Online Library for rules of use; OA articles are governed by the applicable Creative Commons License

19448007, 2026, 20, Downloaded from https://agupubs.onlinelibrary.wiley.com/doi/10.1029/2026GL124581, Wiley Online Library on [18/10/2026]. See the Terms and Conditions (https://onlinelibrary.wiley.com/terms-and-conditions) on Wiley Online Library for rules of use; OA articles are governed by the applicable Creative Commons License

The T2 (171–211 cm; 34,231 ± 270 ^{14}C yr BP) and T5 (29–45 cm; 8,240 ± 30 ^{14}C yr BP) layers developed a clear coarsening-to-fining upward grading (Figure 2g). Furthermore, the bases of T2 and T5 are marked by abrupt shifts in sorting coefficient (Figure S3 in Supporting Information S1), coupled with a notable increase in calcareous detritus (Figures S4 and S5 in Supporting Information S1), which leads us to interpret these layers as a single-phase STC deposit. The T1 (249–267 cm; 38,762 ± 910 ^{14}C yr BP) and T4 (53–89 cm; 27,451 ± 130 ^{14}C yr BP) layers comprise individual units that resemble the single-phase STC layers in internal structure and elemental signature, but each unit was almost immediately eroded and overlain by subsequent coarse-grained sediment inputs (Figure 2g; Figures S3 in Supporting Information S1). This recurrent pattern argues that these layers can be identified as multi-phase STC layers. The T3 (123–139 cm; 35,075 ± 920 ^{14}C yr BP), exhibiting a reverse grading, showing an upward-coarsening trend and well-defined basal lamination (Figure 2g; Figure S1 in Supporting Information S1), can be interpreted as an inversely graded STC layer (Mulder et al., 2001). The intervals without turbidites are characterized by relatively stable sedimentation, uniform color, homogeneous composition, and well-developed horizontal laminations, which are collectively interpreted as hemipelagic layers (Figures 2f–2g, Figures S1 and S3–S5 in Supporting Information S1).

Overall, the hemipelagic layers exhibit high TOC content, enriched $\delta^{13}C_{TOC}$ values, and fine particles, which differ significantly from the STC layers in OC characteristics and sediment properties ($p < 0.05$). The sediments deposited during each STC event have a lower TOC content (0.3 ± 0.1 wt.%; $n = 73$) compared to the hemipelagic layers (0.4 ± 0.1 wt.%; $n = 73$; Figure 2a; Figure S6 in Supporting Information S1) ($p < 0.05$). The STC layers are more enriched in $\delta^{13}C_{TOC}$ (−21.9‰ ± 0.4‰) and have a significantly higher C/N value (7.5 ± 1.0) than that of the hemipelagic layer (−22.0‰ ± 0.5‰ and 6.8 ± 0.9; Figure 2a; Figure S6 in Supporting Information S1) ($p < 0.05$). Notably, the hemipelagic layer in 223–247 cm comprises the oldest sediment (about 40,068 ± 410 ^{14}C yr BP), which characterizes the lowest TOC content (0.2 ± 0.1 wt.%) (Figure 2a and Figure S7 in Supporting Information S1). We attribute this geochemical discrepancy to sea-level lowering at ∼40 kyr BP, which led to a sharp increase in terrestrial input and oxygen-exposure degradation of OC (Lambeck et al., 2014; Liu et al., 2009).

A comparison of the sediment and OC characteristics reveals that slope sediments possess finer grain sizes, higher OC contents, and more pronounced marine signatures than shelf sediments (Lin et al., 2024; Figure S8 in Supporting Information S1). The limited association between OC and protective clay minerals on the northern shelf leads to poor OC preservation, thereby explaining the lower TOC content in shelf sediments (Lin et al., 2024). This difference is also evident in the hemipelagic and STC layers, and we therefore infer that they have distinct sediment and OC sources, corroborating earlier studies on STC provenance in this region (Li et al., 2017). The fine particles exhibiting high TOC content and marine signatures in hemipelagic layer sediments indicate the presence of autochthonous OC derived from prevailing depositional processes on the continental slope (Figure S8 in Supporting Information S1). The distinct sedimentary textures, mineralogical compositions, and OC properties suggest that the contribution of OC eroded from the northern continental shelf is minimal (Figure 2; Figure S4 in Supporting Information S1). The foraminifera-rich sandy sediment textures and pronounced terrestrial signatures indicate that STC transports sediment and OC from the northern shelf to the slope, thereby contributing to layers that exhibit shelf characteristics (Li et al., 2017; Figures 1c, 2a and 2g).

3.2. Characteristics of Fe-OC in STC Deposits

Fe_R content declines markedly with increasing depth across the upper core interval (0–27 cm) (Figure 2c). With increasing burial depth, the shift from oxic to anoxic conditions induces Fe_R reduction (Y. Hu et al., 2025). Below this layer, the Fe_R content remains relatively stable with a mean of 19.2 ± 5.0 μmol g^{-1} (Figure 2c). Overall, the hemipelagic layers exhibit the similar Fe-OC content (0.1 ± 0.0 wt.%) and lower $f_{Fe\text{-}OC}$ (18.0 ± 5.5%) compared to all layers (0.1 ± 0.0 wt.% and 20.2 ± 7.0%; Figures 2b and 2d) ($p < 0.05$). Particularly, the layer in 223–247 cm comprises coarser sediment than other hemipelagic layers (Figure 2g) ($p < 0.05$), which characterizes the low Fe-OC content (0.05 ± 0.01 wt.%) but high $f_{Fe\text{-}OC}$ (22.1 ± 3.5%) (Table S4 in Supporting Information S1; Figures 2d and 2e). The increase in terrestrial input and OC re-oxidation during this period probably caused the discrepancy (Lambeck et al., 2014; Liu et al., 2009). Compared to the slope surface sediments (Figure S8 in Supporting Information S1), the hemipelagic deposits exhibited a more enriched $\delta^{13}C_{Fe\text{-}OC}$ ($p < 0.05$), and a comparable $f_{Fe\text{-}OC}$ and OC/Fe ratio ($p > 0.05$). We therefore propose that during the background deposition and burial, labile OC from plant and soil sources associated with Fe_R is progressively stripped away and preferentially degraded.

19448007, 2026, 20, Downloaded from https://agupubs.onlinelibrary.wiley.com/doi/10.1029/2026GL124581, Wiley Online Library on [18/10/2026]. See the Terms and Conditions (https://onlinelibrary.wiley.com/terms-and-conditions) on Wiley Online Library for rules of use; OA articles are governed by the applicable Creative Commons License

The STC deposits exhibit distinct variations in Fe-OC content and $f_{Fe\text{-}OC}$ during the deposition processes (Figures 2b and 2d). Although the Fe-OC contents in the STC layers are relatively low (0.1 ± 0.0 wt.%), the $f_{Fe\text{-}OC}$ attains 22.1 ± 7.6% (Table S4 in Supporting Information S1), comparable to the average value of global marine surface sediments (21.5% ± 8.6%; Lalonde et al., 2012). The $f_{Fe\text{-}OC}$ gradually decreases along the upwardly tapering positive grain sequence in a single STC event, suggesting that the variation in the Fe-OC role is closely linked to the STC process (Figure 2d; Figure S9 in Supporting Information S1). Additionally, the variations in $\delta^{13}C_{Fe\text{-}OC}$ value and OC/Fe ratio also respond to the STC process (Figures 2b and 2e), thus consistently confirming that the STC process modifies the source and formation mechanism of Fe-OC. On the one hand, the STC layers exhibit a markedly higher $f_{Fe\text{-}OC}$ and OC/Fe ratio relative to hemipelagic layers ($p < 0.05$) (Figure S8 in Supporting Information S1), which shows that Fe_R in STC layers exhibits stronger OC binding capacity and greater resistance to degradation.

On the other hand, the STC deposits exhibited a similar $f_{Fe\text{-}OC}$ and more enriched $\delta^{13}C_{Fe\text{-}OC}$ ($p < 0.05$), compared to the shelf surface sediments (Figure S8 in Supporting Information S1). Although degradation can result in isotope fractionation, we contend that the impact of this fractionation is minimal in the context of the rapid STC processes (Freudenthal et al., 2001). Based on this, we hypothesize that the erosion and transport disrupted the redox conditions on the shelf, leading to the loss of the terrestrial Fe-OC signature. Nevertheless, the preference for the co-precipitation binding mechanism strengthened associations between Fe_R and OC, according to high OC/Fe (Figure 2e). Moreover, the sandy sedimentary environment facilitates the re-oxidation of iron, allowing for the capture of more refractory OC from the water column and porewater (Burdige & Komada, 2025; Xiao et al., 2025). Oxygen vacancy defects generated in oxidized Fe_R phases (e.g., hematite) can substantially accelerate the Maillard reaction and transform OC into structurally stable and complex compounds (Nie et al., 2026). TGA analysis supporting this hypothesis reveals that the Fe-OC in STC deposits exhibits higher thermal stability than that in hemipelagic deposits ($p < 0.05$), particularly within the T2 and T5 single-phase STC layers (Figures S10a and S10b in Supporting Information S1). Furthermore, pronounced heterogeneity in Fe-OC thermal stability within individual turbidite beds, with the highest stability consistently found in the coarse-grained top deposits of the STC (Figure S10a in Supporting Information S1). Thus, the $f_{Fe\text{-}OC}$ maintains its quantity but experiences a qualitative shift toward greater thermal stability during the STC processes.

Collectively, STC also exerts a double-edged influence on the rusty carbon sink, as this vigorous dynamic process may accelerate the degradation of labile OC from river inputs (Bao, van der Voort, et al., 2018), thereby weakening the capacity of Fe-OC to preserve this labile fraction. Nevertheless, the burial of refractory Fe-OC extends the OC turnover on the slope, allowing it to enter the geological cycle and making this region a long-term carbon sink. Furthermore, the buried Fe-OC then provides essential substrates for subsurface microbial communities and fuels subsequent deep C-Fe-S reactions (Chu et al., 2023; Martindale et al., 2025).

3.3. Efficient Accumulation of Fe-OC in STC Deposits

To estimate the role of STC deposits in the Fe-OC accumulation, we combined measured TOC content, $f_{Fe\text{-}OC}$, and dry bulk density in the core. The accumulation rates for hemipelagic layers were calculated from measured sedimentation rates, while those for STC layers were determined by integration of the OC density distribution per event (Text S8). Driven by rapid transport, the accumulation rates of TOC and Fe-OC across the STC layers are as high as 889.8 ± 519.9 and 185.4 ± 84.6 g m^{-2} $time^{-1}$, respectively (Table S7 in Supporting Information S1). In contrast, the accumulation rates of TOC and Fe-OC across the hemipelagic layers are only 0.3 ± 0.3 and 0.1 ± 0.1 g m^{-2} yr^{-1}, respectively (Table S7 in Supporting Information S1). Owing to the persistence time of merely hours up to a maximum of several days (Talling et al., 2022), STC events exhibit high instantaneous carbon accumulation and burial potential. Per-event TOC and Fe-OC accumulation within STC deposits is three to four orders of magnitude higher than annual hemipelagic accumulation in hemipelagic layers (Figure 3a) ($p < 0.05$). Over the about 40 kyr depositional record of core Q11, the carbon stock in STC deposits accounts for 44.4% and 49.3% of the total OC and Fe-OC stock, respectively (Figure 3b).

We present compelling evidence supporting the integration of STC systems into global Fe-OC burial budgets through expanding the global Fe-OC accumulation data set by providing new geochemical information (see methods) (Figure 3c; Table S8 in Supporting Information S1). The $f_{Fe\text{-}OC}$ in STC deposits exhibits the highest value among sedimentary carbon sinks (Figure 3d) ($p < 0.05$). Coastal wetlands harbor substantial Fe-OC content, with $f_{Fe\text{-}OC}$ averaging 15.7% ± 9.3% (Table S9 in Supporting Information S1), driven by substantial

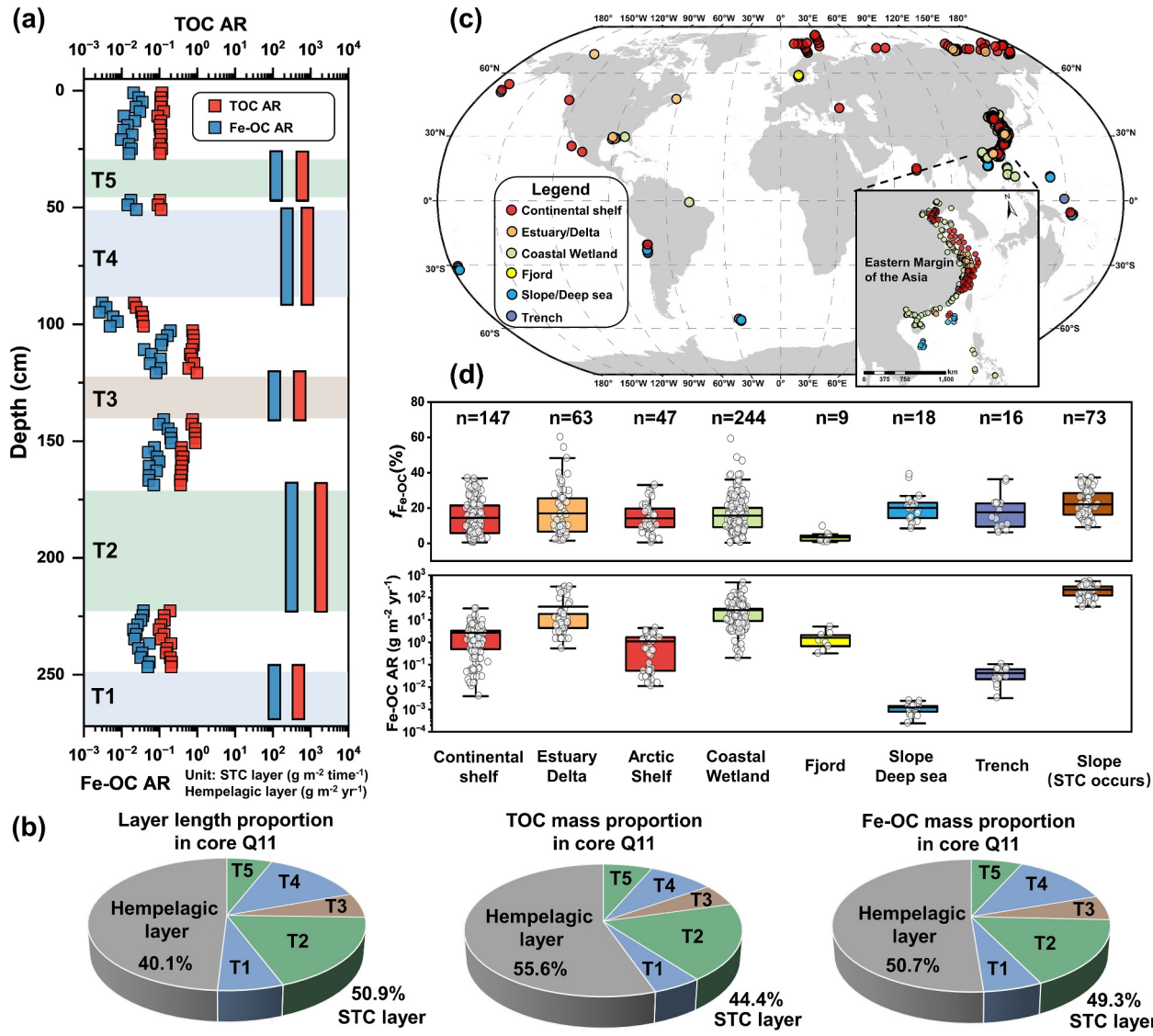

Figure 3. The total organic carbon (TOC) and Fe-OC accumulation rate in core Q11 and other different sedimentary carbon sinks. (a) The TOC and Fe-OC accumulation rate in core Q11. The accumulation rate of each sandy turbidity current (STC) layer is quantified by integrating the organic carbon density distribution, with only one accumulation rate obtained per event. Different colors of dark backgrounds represent different types of STC event deposit layers. (b) The layer length, TOC mass, and Fe-OC mass proportion of the hemipelagic and STC layer in core Q11. (c) The global distribution of Fe-OC proportion and Fe-OC accumulation rate calculated from literature data in different sedimentary carbon sinks; (d) The statistical analysis of Fe-OC proportion and Fe-OC accumulation rate across different sedimentary carbon sinks.

plant-derived OC inputs and tidal activity (Ma et al., 2025). The $f_{\text{Fe-OC}}$ in shallow nearshore settings is comparable to that in coastal wetlands: estuarine deltas, the continental shelf, and the permafrost-affected Arctic shelf exhibit values of 17.0% ± 13.7%, 14.1% ± 9.3%, and 14.2% ± 7.8%, respectively (Figure 4c; Table S9 in Supporting Information S1). The $f_{\text{Fe-OC}}$ in deep-water settings (excluding fjords) shows a moderately higher value than shallow near-shore settings, with a mean of 20.1% ± 8.1% on slopes and abyssal plains, and 17.6% ± 9.1% in trenches (Figure 3d; Table S9 in Supporting Information S1) ($p < 0.05$).

The Fe-OC accumulation rate on the continental slope where STC deposits occur is more than approximately 7 times higher than that in coastal wetlands (27.4 ± 41.2 g m^{-2} yr^{-1}) and estuarine deltas (39.0 ± 78.5 g m^{-2} yr^{-1}), and over 100 times higher than that in continental shelves (2.7 ± 4.3 g m^{-2} yr^{-1}) (Figure 3d; Tables S7 and S9 in Supporting Information S1) ($p < 0.05$). These regions are traditionally recognized as hotspots for Fe-OC burial, due to their substantial receipt of terrestrial material and high sediment accumulation rates (Longman et al., 2022;

19448007, 2026, 20, Downloaded from https://agupubs.onlinelibrary.wiley.com/doi/10.1029/2026GL124581, Wiley Online Library on [18/10/2026]. See the Terms and Conditions (https://onlinelibrary.wiley.com/terms-and-conditions) on Wiley Online Library for rules of use; OA articles are governed by the applicable Creative Commons License

10.1029/2026GL124581

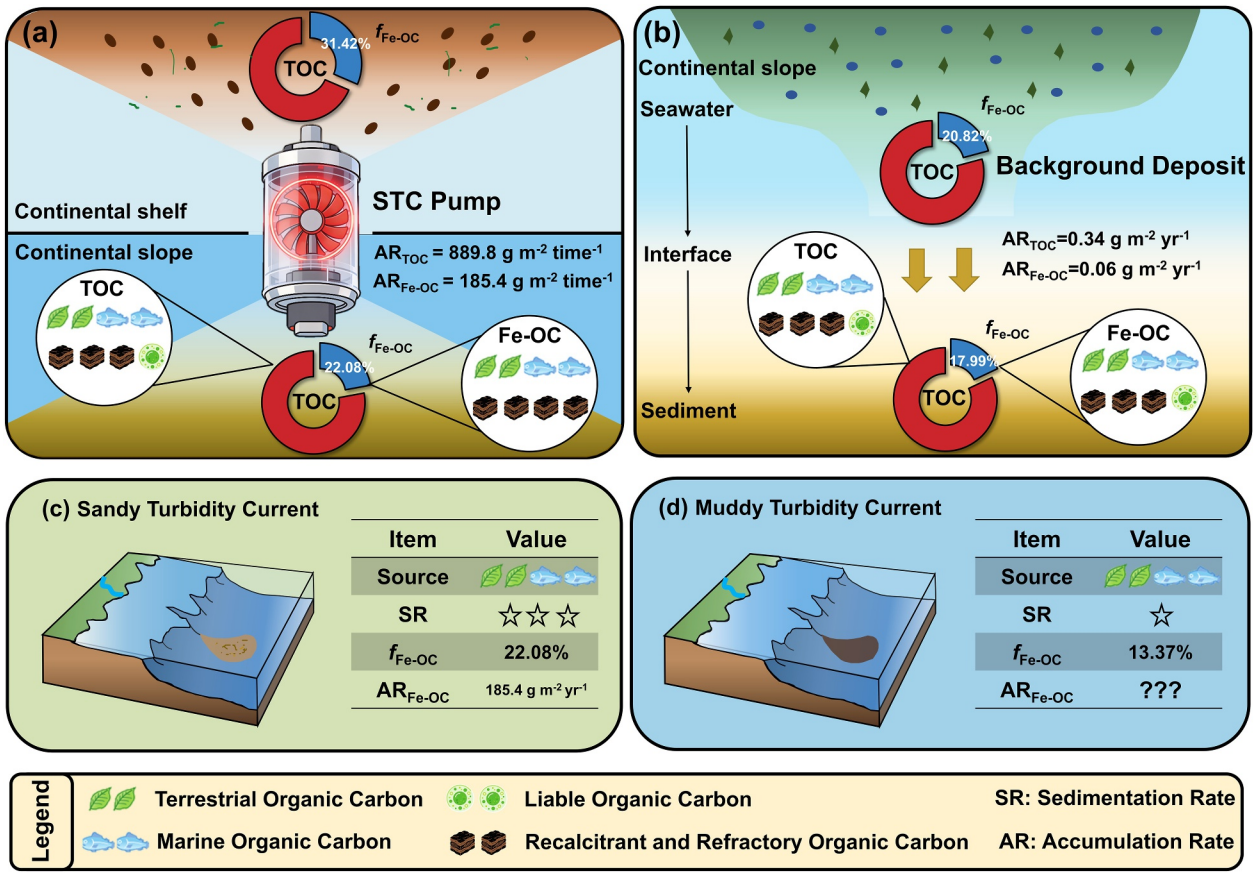

Figure 4. The different paradigms between the sandy turbidity current (STC) pump and background deposit (hemipelagic deposit) at the shelf edge, and different types of turbidity current systems: (a) The paradigm of STC pump; (b) The paradigm of background deposit (hemipelagic deposit); Carbon pump function in different types of turbidity current system: (c) STC that is at the shelf edge; (d) muddy turbidity current (MTC) that is at the shelf edge. The f_{Fe-OC} data in the MTC deposit are derived from Z. Zhang, Lu, et al. (2024), Z. Zhang, Zhang, et al. (2024).

Zhao et al., 2018). Moreover, in contrast to the depositional modes in these regions, STC rapidly transports Fe-OC into slope sediments, thereby minimizing OC degradation and thus achieving highly efficient sequestration (Baker et al., 2024; Hage et al., 2020). Despite fjords and deep-sea trenches sharing similarly efficient burial of Fe-OC (Bao, Strasser, et al., 2018; Smith et al., 2015), our results show that these two regions exhibit relatively low Fe-OC accumulation rates (Figure 4d; Table S9 in Supporting Information S1) ($p < 0.05$), probably attributable to limited Fe-OC source and inputs (Bao, Strasser, et al., 2018; Placitu et al., 2024).

Despite the significantly lower area of STC deposits in the slope compared to coastal wetlands, continental shelves, and the pelagic ocean (Talling et al., 2024; Yool & Fasham, 2001), we rank them as one of the important hotspots for Fe-OC burial in the sedimentary carbon system, based on the mass of Fe-OC buried per unit area. In addition, TGA analysis suggests that the majority of buried OC and Fe-OC is refractory (Figure S10 in Supporting Information S1), likely derived from fossil OC in weathered bedrock, terrestrial soil, and black carbon (Lopez-Capel et al., 2005). The high thermal stability of Fe-OC in STC deposits may represent a different accumulation effect, contrasting with the biospheric OC sequestration effects in coastal and shallow nearshore regions (Figure 3c; Galy et al., 2007; Hage et al., 2020). Therefore, the STC events, especially the large-scale deposits, function as an efficient transfer pump of refractory Fe-OC across the global sedimentary carbon systems (Figure 4a). Continental slopes emerge as a potential and stable sink for Fe-OC, which has often been overlooked.

3.4. Implications for the Carbon Cycle

Our findings corroborate the dual effects of STC in shaping Fe-OC characteristics of slope sediments. One is a "space shuttle" effect: STC rapidly transports Fe-OC from shelf sediments into the slope environment. This rapid

19448007, 2026, 20, Downloaded from https://agupubs.onlinelibrary.wiley.com/doi/10.1029/2026GL124581, Wiley Online Library on [18/10/2026]. See the Terms and Conditions (https://onlinelibrary.wiley.com/terms-and-conditions) on Wiley Online Library for rules of use; OA articles are governed by the applicable Creative Commons License

19448007, 2026, 20, Downloaded from https://agupubs.onlinelibrary.wiley.com/doi/10.1029/2026GL124581, Wiley Online Library on [18/10/2026]. See the Terms and Conditions (https://onlinelibrary.wiley.com/terms-and-conditions) on Wiley Online Library for rules of use; OA articles are governed by the applicable Creative Commons License

process delivers Fe-OC with distinct compositional characteristics, largely bypassing the degradation that would occur during background sedimentation (Figures 4a and 4b; Hage et al., 2020; Talling et al., 2024). The second is the "trap effect": STC generates coarse-grained and oxygenated sedimentary environment, facilitating the formation of poorly crystalline iron oxides (Zhou et al., 2024). The poorly crystalline Fe_R capture refractory dissolved OC (e.g., aromatic compounds) from the water column and porewater to form highly stable Fe-OC (Burdige & Komada, 2025; Xiao et al., 2025). Unlike biospheric OC, whose long-term preservation hinges on sustained anoxic conditions, the refractory Fe-OC delivered by STC relies on its intrinsic chemical recalcitrance and mineral-binding state (Faust et al., 2021; Hemingway et al., 2019; Moore et al., 2023). The Fe-OC maintains considerable stability even through redox fluctuations induced by early diagenesis, achieving genuine "geological sequestration" (Chen et al., 2024; Y. Hu et al., 2025).

Documented evidence shows that STC has been prevalent on continental shelf edges globally across geological history (Amaro et al., 2016; Hage et al., 2020; Talling et al., 2024). Its mechanism is likely operative in, and critically important for, carbon sequestration in major STC-prone settings worldwide, including the SCS, Arctic shelf, and the Amazon shelf, etc. (Hilton et al., 2015; Li et al., 2017; Nittrouer et al., 2021). Therefore, integrating the STC rusty carbon pump into the global carbon cycle models could substantially enhance the robustness of both carbon cycle projections and climate change forecasts. We also point out several questions that remain unresolved, particularly concerning how different types of turbidity currents influence the Fe-OC properties (Figures 4c and 4d), and the specific mechanisms of Fe_R and OC interaction during turbidity current events. The proportion of Fe-OC varies considerably among depositional settings (Figures 4c and 4d). Muddy turbidity current (MTC) deposits feature low permeability and undergo oxidative degradation upon resuspension, restricting Fe_R re-oxidation and thus reducing the efficiency of Fe-OC formation (Z. Zhang, Lu, et al., 2024; Z. Zhang, Zhang, et al., 2024; Zhao et al., 2018). Accordingly, we speculate that the rusty carbon pump operates more efficiently in STC, whereas MTC relies more on mineral physical shielding instead of active iron-cycling. The quantitative and qualitative implications of this previously unexplained global carbon pump mechanism should be further explored, alongside a re-evaluation of OC sequestration potential at shelf edges.

Conflict of Interest

The authors declare no conflicts of interest relevant to this study.

Availability Statement

The data reported in this study are available at Zou (2026). We also temporarily uploaded a copy of our data as Supporting Information S1 for review purposes.

Acknowledgments
This work was supported by the Natural Science Foundation of China (Grant 42576210, 92358301), the Innovation Project of Natural Resources Science and Technology of Jiangsu Province (JSZRKJ202423), and the Fundamental Research Funds for the Central Universities (Grants 0209-14380134, 0209-14380162, and 0209-14370414). We gratefully acknowledge Cruise NORC2019-06, carried out by the R/V Xiangyanghong 18 in the South China Sea in August 2020, for providing the sediment samples used in this study. We sincerely thank the handling Editor and two reviewers for carefully evaluating our manuscript and providing thoughtful, constructive comments. Their valuable suggestions have substantially improved the quality, clarity, and rigor of this study.

References

Amaro, T., Huvenne, V. A. I., Allcock, A. L., Aslam, T., Davies, J. S., Danovaro, R., et al. (2016). The Whittard Canyon–A case study of submarine canyon processes. *Progress in Oceanography*, *146*, 38–57. https://doi.org/10.1016/j.pocean.2016.06.003

Baker, M. L., Hage, S., Talling, P. J., Acikalin, S., Hilton, R. G., Haghipour, N., et al. (2024). Globally significant mass of terrestrial organic carbon efficiently transported by canyon-flushing turbidity currents. *Geology*, *52*(8), 6–636. https://doi.org/10.1130/g51976.1

Bao, R., Strasser, M., McNichol, A. P., Haghipour, N., McIntyre, C., Wefer, G., & Eglinton, T. I. (2018). Tectonically-triggered sediment and carbon export to the Hadal zone. *Nature Communications*, *9*(1), 121. https://doi.org/10.1038/s41467-017-02504-1

Bao, R., van der Voort, T. S., Zhao, M., Guo, X., Montluçon, D. B., McIntyre, C., & Eglinton, T. I. (2018). Influence of hydrodynamic processes on the fate of sedimentary organic matter on Continental margins. *Global Biogeochemical Cycles*, *32*(9), 1420–1432. https://doi.org/10.1029/2018gb005921

Berner, R. A. (1982). Burial of organic carbon and pyrite sulfur in the modern ocean: Its geochemical and environmental significance. *American Journal of Science*, *282*, 451–473.

Bernhardt, A., & Schwanghart, W. (2025). Seafloor slopes control submarine canyon distribution: A global analysis. *Science Advances*, *11*(24), eadv3942. https://doi.org/10.1126/sciadv.adv3942

Bianchi, T. S., Cui, X., Blair, N. E., Burdige, D. J., Eglinton, T. I., & Galy, V. (2018). Centers of organic carbon burial and oxidation at the land-ocean interface. *Organic Geochemistry*, *115*, 138–155. https://doi.org/10.1016/j.orggeochem.2017.09.008

Burdige, D. J. (2007). Preservation of organic matter in marine sediments: Controls, mechanisms, and an imbalance in sediment organic carbon budgets? *Chemical Reviews*, *107*(2), 467–485.

Burdige, D. J., & Komada, T. (2025). Organic carbon cycling in hemipelagic and turbidite sediments of Santa Monica Basin, California Borderland. *Geochimica et Cosmochimica Acta*, *415*, 252–265. https://doi.org/10.1016/j.gca.2025.12.053

Chen, Y., Dong, L., Sui, W., Niu, M., Cui, X., Hinrichs, K. U., & Wang, F. (2024). Cycling and persistence of iron-bound organic carbon in subseafloor sediments. *Nature Communications*, *15*(1), 6370. https://doi.org/10.1038/s41467-024-50578-5

Chen, Y., & Wang, F. (2026). Dynamic roles of reactive iron in organic carbon preservation in marine sediments. *Fundamental Research*. https://doi.org/10.1016/j.fmre.2026.04.004

Chu, M., Liu, J., Li, H., Zhou, Y., Wang, N., Xia, C., et al. (2023). Earthquake-induced redistribution and reburial of microbes in the hadal trenches. *The Innovation Geoscience*, *1*(2), 100027. https://doi.org/10.59717/j.xinn-geo.2023.100027

Dennielou, B., Droz, L., Babonneau, N., Jacq, C., Bonnel, C., Picot, M., et al. (2017). Morphology, structure, composition and build-up processes of the active channel-mouth lobe complex of the Congo deep-sea fan with inputs from remotely operated underwater vehicle (ROV) multibeam and video surveys. *Deep Sea Research Part II: Topical Studies in Oceanography*, *142*, 25–49. https://doi.org/10.1016/j.dsr2.2017.03.010

Faust, J. C., Tessin, A., Fisher, B. J., Zindorf, M., Papadaki, S., Hendry, K. R., et al. (2021). Millennial scale persistence of organic carbon bound to iron in Arctic marine sediments. *Nature Communications*, *12*(1), 275. https://doi.org/10.1038/s41467-020-20550-0

Freudenthal, T., Wagner, T., Wenzhöfer, F., Zabel, M., & Wefer, G. (2001). Early diagenesis of organic matter from sediments of the eastern subtropical Atlantic: Evidence from stable nitrogen and carbon isotopes. *Geochimica et Cosmochimica Acta*, *65*(11), 1795–1808. https://doi.org/10.1016/s0016-7037(01)00554-3

Galy, V., France-Lanord, C., Beyssac, O., Faure, P., Kudrass, H., & Palhol, F. (2007). Efficient organic carbon burial in the Bengal fan sustained by the Himalayan erosional system. *Nature*, *450*(7168), 407–410. https://doi.org/10.1038/nature06273

Galy, V., Peucker-Ehrenbrink, B., & Eglinton, T. (2015). Global carbon export from the terrestrial biosphere controlled by erosion. *Nature*, *521*(7551), 204–207. https://doi.org/10.1038/nature14400

Gao, S., Zhuo, H., Wang, Y., Wang, X., Jia, K., & Zhou, W. (2019). Sedimentary features and genetic mechanisms of the Foraminifera rich sand layers in the modern Baiyun submarine canyons, Northern South China Sea. *Acta Sedimentologica Sinica*, *37*, 798–811.

Hage, S., Galy, V. V., Cartigny, M. J. B., Acikalin, S., Clare, M. A., Gröcke, D. R., et al. (2020). Efficient preservation of young terrestrial organic carbon in sandy turbidity-current deposits. *Geology*, *48*(9), 882–887. https://doi.org/10.1130/g47320.1

Hage, S., Romans, B. W., Peploe, T. G., Poyatos-Moré, M., Haeri Ardakani, O., Bell, D., et al. (2022). High rates of organic carbon burial in submarine deltas maintained on geological timescales. *Nature Geoscience*, *15*(11), 919–924. https://doi.org/10.1038/s41561-022-01048-4

Hedges, J. I., Keil, R. G., & Benner, R. (1997). What happens to terrestrial organic matter in the ocean? *Organic Geochemistry*, *27*(5–6), 195–212. https://doi.org/10.1016/s0146-6380(97)00066-1

Hemingway, J. D., Rothman, D. H., Grant, K. E., Rosengard, S. Z., Eglinton, T. I., Derry, L. A., & Galy, V. V. (2019). Mineral protection regulates long-term global preservation of natural organic carbon. *Nature*, *570*(7760), 228–231. https://doi.org/10.1038/s41586-019-1280-6

Hilton, R. G., Galy, V., Gaillardet, J., Dellinger, M., Bryant, C., O'Regan, M., et al. (2015). Erosion of organic carbon in the Arctic as a geological carbon dioxide sink. *Nature*, *524*(7563), 84–87. https://doi.org/10.1038/nature14653

Hu, L., Ji, Y., Zhao, B., Liu, X., Du, J., Liang, Y., & Yao, P. (2023). The effect of iron on the preservation of organic carbon in marine sediments and its implications for carbon sequestration. *Science China Earth Sciences*, *66*(9), 1946–1959. https://doi.org/10.1007/s11430-023-1139-9

Hu, Y., Li, K., Faust, J. C., Peckmann, J., Zhang, D., Chen, L., et al. (2025). Stability of reactive iron-bound organic carbon during sulfidization of iron oxides: Insights from methane-seep sediments. *Geophysical Research Letters*, *52*(8), e2024GL112119. https://doi.org/10.1029/2024gl112119

Jokinen, S., Koho, K., Virtasalo, J., & Jilbert, T. (2020). Sedimentary molybdenum and uranium sequestration in a non-euxinic coastal setting: Role of the sulfate-methane transition zone (no. EGU2020-12973). In *Copernicus meetings*.

Kao, S. J., Hilton, R. G., Selvaraj, K., Dai, M., Zehetner, F., Huang, J. C., et al. (2014). Preservation of terrestrial organic carbon in marine sediments offshore Taiwan: Mountain building and atmospheric carbon dioxide sequestration. *Earth Surface Dynamics*, *2*(1), 127–139. https://doi.org/10.5194/esurf-2-127-2014

Lalonde, K., Mucci, A., Ouellet, A., & Gélinas, Y. (2012). Preservation of organic matter in sediments promoted by iron. *Nature*, *483*(7388), 198–200. https://doi.org/10.1038/nature10855

Lambeck, K., Rouby, H., Purcell, A., Sun, Y., & Sambridge, M. (2014). Sea level and global ice volumes from the Last Glacial Maximum to the Holocene. *Proceedings of the National Academy of Sciences*, *111*(43), 15296–15303. https://doi.org/10.1073/pnas.1411762111

Lee, H., Galy, V., Feng, X., Ponton, C., Galy, A., France-Lanord, C., & Feakins, S. J. (2019). Sustained wood burial in the Bengal Fan over the last 19 My. *Proceedings of the National Academy of Sciences*, *116*(45), 22518–22525. https://doi.org/10.1073/pnas.1913714116

Li, N., Feng, D., Chen, L., Wang, H., & Chen, D. (2017). Compositions of foraminifera-rich turbidite sediments from the Shenhu area on the northern slope of the South China Sea: Implication for the presence of deep water bottom currents. *Journal of Asian Earth Sciences*, *138*, 148–160. https://doi.org/10.1016/j.jseaes.2017.02.010

Lin, B., Liu, Z., Eglinton, T. I., Wiesner, M. G., Blattmann, T. M., & Haghipour, N. (2024). Organic carbon sources in surface sediments on the northern South China Sea. *Journal of Geophysical Research: Biogeosciences*, *129*(4), e2023JG007909. https://doi.org/10.1029/2023jg007909

Liu, Z., Zhao, Y., Colin, C., Siringan, F. P., & Wu, Q. (2009). Chemical weathering in Luzon, Philippines from clay mineralogy and major-element geochemistry of river sediments. *Applied Geochemistry*, *24*(11), 2195–2205. https://doi.org/10.1016/j.apgeochem.2009.09.025

Longman, J., Faust, J. C., Bryce, C., Homoky, W. B., & März, C. (2022). Organic carbon burial with reactive iron across global environments. *Global Biogeochemical Cycles*, *36*(11), e2022GB007447. https://doi.org/10.1029/2022gb007447

Lopez-Capel, E., Sohi, S. P., Gaunt, J. L., & Manning, D. A. C. (2005). Use of thermogravimetry–differential scanning calorimetry to characterize modelable soil organic matter fractions. *Soil Science Society of America Journal*, *69*(1), 136–140. https://doi.org/10.2136/sssaj2005.0136a

Ma, H., Thompson, A., Hall, S. J., Wang, J., Xiao, Y., Liu, C. Q., & Chen, C. (2025). Enrichment of metastable iron minerals in global coastal wetlands. *Nature Geoscience*, *18*(9), 885–892. https://doi.org/10.1038/s41561-025-01764-7

Martindale, R. C., Sinha, S., Stone, T. N., Fonville, T., Bodin, S., Krencker, F. N., & Kabiri, L. (2025). Chemosynthetic microbial communities formed wrinkle structures in ancient turbidites.

Miao, X., Wei, J., Liu, X., Qiao, X., & Li, J. (2023). The control of turbidite deposition on pyrite sulfur isotopic composition in sediments on the continental slope of the South China Sea. *Marine Geology*, *465*, 107163. https://doi.org/10.1016/j.margeo.2023.107163

Moore, O. W., Curti, L., Woulds, C., Bradley, J. A., Babakhani, P., Mills, B. J., et al. (2023). Long-term organic carbon preservation enhanced by iron and manganese. *Nature*, *621*(7978), 312–317. https://doi.org/10.1038/s41586-023-06325-9

Mulder, T., Migeon, S., Savoye, B., & Faugères, J. C. (2001). Inversely graded turbidite sequences in the deep Mediterranean: A record of deposits from flood-generated turbidity currents? *Geo-Marine Letters*, *21*(2), 86–93.

Nie, S., Yu, W., Zhu, X., Liu, L., Wang, J., Xiao, X., & Chen, B. (2026). Oxygen vacancy defects in Hematite enhance maillard reactions and promote recalcitrant organic carbon Formation. *Environmental Science & Technology*.

Nittrouer, C. A., DeMaster, D. J., Kuehl, S. A., Jr Figueiredo, A. G., Sternberg, R. W., Faria, L. E. C., et al. (2021). Amazon sediment transport and accumulation along the continuum of mixed fluvial and marine processes. *Annual Review of Marine Science*, *13*(1), 501–536. https://doi.org/10.1146/annurev-marine-010816-060457

Placitu, S., van de Velde, S. J., Hylén, A., Hall, P. O. J., Robertson, E. K., Eriksson, M., et al. (2024). Limited organic carbon burial by the rusty carbon sink in Swedish fjord sediments. *Journal of Geophysical Research: Biogeosciences*, *129*(11), e2024JG008277. https://doi.org/10.1029/2024jg008277

19448007, 2026, 20, Downloaded from https://agupubs.onlinelibrary.wiley.com/doi/10.1029/2026GL124581, Wiley Online Library on [18/10/2026]. See the Terms and Conditions (https://onlinelibrary.wiley.com/terms-and-conditions) on Wiley Online Library for rules of use; OA articles are governed by the applicable Creative Commons License

Shields, M. R., Bianchi, T. S., Gélinas, Y., Allison, M. A., & Twilley, R. R. (2016). Enhanced terrestrial carbon preservation promoted by reactive iron in deltaic sediments. *Geophysical Research Letters*, *43*(3), 1149–1157. https://doi.org/10.1002/2015gl067388

Smith, R. W., Bianchi, T. S., Allison, M., Savage, C., & Galy, V. (2015). High rates of organic carbon burial in fjord sediments globally. *Nature Geoscience*, *8*(6), 450–453. https://doi.org/10.1038/ngeo2421

Talling, P. J., Baker, M. L., Pope, E. L., Ruffell, S. C., Jacinto, R. S., Heijnen, M. S., et al. (2022). Longest sediment flows yet measured show how major rivers connect efficiently to deep sea. *Nature Communications*, *13*(1), 4193. https://doi.org/10.1038/s41467-022-31689-3

Talling, P. J., Hage, S., Baker, M. L., Bianchi, T. S., Hilton, R. G., & Maier, K. L. (2024). The global turbidity current pump and its implications for organic carbon cycling. *Annual Review of Marine Science*, *16*(1), 105–133. https://doi.org/10.1146/annurev-marine-032223-103626

Tribovillard, N., Algeo, T. J., Lyons, T., & Riboulleau, A. (2006). Trace metals as paleoredox and paleoproductivity proxies: An update. *Chemical Geology*, *232*(1–2), 12–32. https://doi.org/10.1016/j.chemgeo.2006.02.012

Xiao, H., Zhou, Z., Li, J., & Yang, S. (2025). Molecular alteration of dissolved organic matter in intertidal sediments: The role of Fe (II) reoxidation. *Environmental Science & Technology*.

Yool, A., & Fasham, M. J. (2001). An examination of the "continental shelf pump" in an open ocean general circulation model. *Global Biogeochemical Cycles*, *15*(4), 831–844. https://doi.org/10.1029/2000gb001359

Zhang, Y., Liu, Z., Zhao, Y., Colin, C., Zhang, X., Wang, M., et al. (2018). Long-term in situ observations on typhoon-triggered turbidity currents in the deep sea. *Geology*, *46*(8), 675–678. https://doi.org/10.1130/g45178.1

Zhang, Z., Lu, M., Wang, C., Zhang, C., Lin, B., Liao, Q., et al. (2024). Divergent responses of organic carbon to sedimentary environment transformation in a river-dominated marginal sea. *Journal of Geophysical Research: Biogeosciences*, *129*(11), e2024JG008034. https://doi.org/10.1029/2024jg008034

Zhang, Z., Zhang, C., Qiu, Y., Wang, C., & Zou, X. (2024). The role of reactive iron in the preservation of sedimentary organic carbon in the Pearl River Estuary-northern South China Sea. *Journal of Marine Science*, *43*(4), 151–161.

Zhang, Z., Zhang, C., Qiu, Y., Wang, C., & Zou, X. (2025). The role of reactive iron in preservation of sedimentary organic carbon in the Pearl River Estuary-northern South China Sea. *Journal of Marine Sciences*, *43*(4), 151–161.

Zhao, B., Yao, P., Bianchi, T. S., Shields, M. R., Cui, X., Zhang, X., et al. (2018). The role of reactive iron in the preservation of terrestrial organic carbon in estuarine sediments. *Journal of Geophysical Research: Biogeosciences*, *123*(12), 3556–3569. https://doi.org/10.1029/2018jg004649

Zhao, B., Yao, P., Bianchi, T. S., Wang, X., Shields, M. R., Schröder, C., & Yu, Z. (2023). Preferential preservation of pre-aged terrestrial organic carbon by reactive iron in estuarine particles and coastal sediments of a large river-dominated estuary. *Geochimica et Cosmochimica Acta*, *345*, 34–49. https://doi.org/10.1016/j.gca.2023.01.023

Zhou, Z., Waska, H., Henkel, S., Dittmar, T., Kasten, S., & Holtappels, M. (2024). Iron promotes the retention of terrigenous dissolved organic matter in subtidal permeable sediments. *Environmental Science & Technology*, *58*(14), 6204–6214. https://doi.org/10.1021/acs.est.3c09531

Zou, X. (2026). Sandy Turbidity Current acts as a Rusty Carbon Pump at the Shelf edge (Version 1) [Dataset]. *Mendeley Data*. https://doi.org/10.17632/38stgsb4h3.1

References From the Supporting Information

Allison, M. A., Bianchi, T. S., McKee, B. A., & Sampere, T. P. (2007). Carbon burial on river-dominated continental shelves: Impact of historical changes in sediment loading adjacent to the Mississippi River. *Geophysical Research Letters*, *34*(1). https://doi.org/10.1029/2006gl028362

Blaauw, M., & Christen, J. A. (2011). Flexible paleoclimate age-depth models using an autoregressive gamma process.

Chaudhary, M. Z., Khan, K., Ahmad, N., Mashiatullah, A., Javed, T., Yaqoob, N., et al. (2021). Sediment accumulation rates in Karachi coastal area Pakistan using ^{210}Pb dating method. *Journal of Radioanalytical and Nuclear Chemistry*, *327*(1), 13–20. https://doi.org/10.1007/s10967-020-07519-5

Chmura, G. L., Anisfeld, S. C., Cahoon, D. R., & Lynch, J. C. (2003). Global carbon sequestration in tidal, saline wetland soils. *Global Biogeochemical Cycles*, *17*(4). https://doi.org/10.1029/2002gb001917

Costa, K. M., Hayes, C. T., Anderson, R. F., Pavia, F. J., Bausch, A., Deng, F., et al. (2020). 230Th normalization: New insights on an essential tool for quantifying sedimentary fluxes in the modern and Quaternary ocean. *Paleoceanography and Paleoclimatology*, *35*(2), e2019PA003820. https://doi.org/10.1029/2019pa003820

Couturier, M., Nozais, C., & Chaillou, G. (2016). Microtidal subterranean estuaries as a source of fresh terrestrial dissolved organic matter to the coastal ocean. *Marine Chemistry*, *186*, 46–57. https://doi.org/10.1016/j.marchem.2016.08.001

Couturier, M., Tommi-Morin, G., Sirois, M., Rao, A., Nozais, C., & Chaillou, G. (2017). Nitrogen transformations along a shallow subterranean estuary. *Biogeosciences*, *14*(13), 3321–3336. https://doi.org/10.5194/bg-14-3321-2017

Díaz-Asencio, M., Herguera, J. C., Romero, F. G., & Rafter, P. (2023). Sediment accumulation rates and carbonate fluxes of deep-sea sediments in the southern Gulf of Mexico. *Marine Geology*, *464*, 107131. https://doi.org/10.1016/j.margeo.2023.107131

Fang, T. H., Chen, J. L., & Huh, C. A. (2007). Sedimentary phosphorus species and sedimentation flux in the East China Sea. *Continental Shelf Research*, *27*(10–11), 1465–1476. https://doi.org/10.1016/j.csr.2007.01.011

Faust, J. C., Stevenson, M. A., Abbott, G. D., Knies, J., Tessin, A., Mannion, I., et al. (2020). Does Arctic warming reduce preservation of organic matter in Barents Sea sediments? *Philosophical Transactions of the Royal Society A: Mathematical, Physical and Engineering Sciences*, *378*(2181), 20190364. https://doi.org/10.1098/rsta.2019.0364

Ghaisas, N. A., Maiti, K., & Roy, A. (2021). Iron-Mediated organic matter preservation in the Mississippi river-influenced shelf sediments. *Journal of Geophysical Research: Biogeosciences*, *126*(4), e2020JG006089. https://doi.org/10.1029/2020jg006089

Jiang, W. (2024). *Preservation of organic carbon byreactive iron in the Hadal Trench (Master dissertation)*. Shanghai Ocean University.

Kuenen, P. H. (1946). Rate and mass of deep-sea sedimentation. *American Journal of Science*, *244*(8), 563–572. https://doi.org/10.2475/ajs.244.8.563

Longman, J., Gernon, T. M., Palmer, M. R., & Manners, H. R. (2021). Tephra deposition and bonding with reactive oxides enhances burial of organic carbon in the Bering Sea. *Global Biogeochemical Cycles*, *35*(11), e2021GB007140. https://doi.org/10.1029/2021gb007140

Ma, W. W., Zhu, M. X., Yang, G. P., & Li, T. (2018). Iron geochemistry and organic carbon preservation by iron (oxyhydr) oxides in surface sediments of the East China Sea and the south Yellow Sea. *Journal of Marine Systems*, *178*, 62–74. https://doi.org/10.1016/j.jmarsys.2017.10.009

Mohamed, C. A. R., Narita, H., Harada, K., & Tsunogai, S. (1996). Sedimentation of natural radionuclides on the seabed across the northern Japan Trench. *Geochemical Journal*, *30*(4), 217–229. https://doi.org/10.2343/geochemj.30.217

Rusakov, V. Y., & Borisov, A. P. (2023). Sedimentation on the Siberian Arctic Shelf as an indicator of the arctic hydrological cycle. *Anthropocene*, *41*, 100370. https://doi.org/10.1016/j.ancene.2023.100370

19448007, 2026, 20, Downloaded from https://agupubs.onlinelibrary.wiley.com/doi/10.1029/2026GL124581, Wiley Online Library on [18/10/2026]. See the Terms and Conditions (https://onlinelibrary.wiley.com/terms-and-conditions) on Wiley Online Library for rules of use; OA articles are governed by the applicable Creative Commons License

Rusakov, V. Y., Tat'yana, G., & Lukmanov, R. A. (2025). Assessment of the sediment budget of the Kara and Laptev seas. *Continental Shelf Research*, *292*, 105506. https://doi.org/10.1016/j.csr.2025.105506

Salvadó, J. A., Tesi, T., Andersson, A., Ingri, J., Dudarev, O. V., Semiletov, I. P., & Gustafsson, Ö. (2015). Organic carbon remobilized from thawing permafrost is resequestered by reactive iron on the Eurasian Arctic Shelf. *Geophysical Research Letters*, *42*(19), 8122–8130. https://doi.org/10.1002/2015gl066058

Sarin, M. M., Borole, D. V., & Krishnaswami, S. (1979). Geochemistry and geochronology of sediments from the Bay of Bengal and the equatorial Indian Ocean. *Proceedings of the Indian Academy of Sciences - Section A*, *88*(13), l–154.

Schuur, E. A., McGuire, A. D., Schädel, C., Grosse, G., Harden, J. W., Hayes, D. J., et al. (2015). Climate change and the permafrost carbon feedback. *Nature*, *520*(7546), 171–179. https://doi.org/10.1038/nature14338

Stuiver, M., & Reimer, P. J. (1993). Extended 14C data base and revised CALIB 3.0 14C age calibration program. *Radiocarbon*, *35*(1), 215–230. https://doi.org/10.1017/s0033822200013904

Sheng, J., Qiao, S., Shi, X., Liu, J., Liu, Y., Liu, S., et al. (2024). Modern sedimentation and sediment budget in the South China Sea and their comparisons with the eastern China seas. *Marine Geology*, *475*, 107348. https://doi.org/10.1016/j.margeo.2024.107348

Sirois, M., Couturier, M., Barber, A., Gelinas, Y., & Chaillou, G. (2018). Interactions between iron and organic carbon in a sandy beach subterranean estuary. *Marine Chemistry*, *202*, 86–96. https://doi.org/10.1016/j.marchem.2018.02.004

Teodoru, C. R., Friedl, G., Friedrich, J., Roehl, U., Sturm, M., & Wehrli, B. (2007). Spatial distribution and recent changes in carbon, nitrogen and phosphorus accumulation in sediments of the Black Sea. *Marine Chemistry*, *105*(1–2), 52–69. https://doi.org/10.1016/j.marchem.2006.12.013

Wang, D., Zhu, M. X., Yang, G. P., & Ma, W. W. (2019). Reactive iron and iron-bound organic carbon in surface sediments of the river-dominated Bohai Sea (China) versus the Southern Yellow Sea. *Journal of Geophysical Research: Biogeosciences*, *124*(1), 79–98. https://doi.org/10.1029/2018jg004722

Wang, X., Li, L., Ren, Y., Cao, P., Zhu, A., Liu, J., & Shi, X. (2023). Early diagenesis and benthic fluxes of redox-sensitive metals in eastern China shelf sediments. *Frontiers in Marine Science*, *10*, 1154248. https://doi.org/10.3389/fmars.2023.1154248

Waterson, E. J., & Canuel, E. A. (2008). Sources of sedimentary organic matter in the Mississippi River and adjacent Gulf of Mexico as revealed by lipid biomarker and δ13CTOC analyses. *Organic Geochemistry*, *39*(4), 422–439. https://doi.org/10.1016/j.orggeochem.2008.01.011

Wu, C. S., Yang, S., Huang, S., & Mu, J. (2016). Delta changes in the Pearl River estuary and its response to human activities (1954–2008). *Quaternary International*, *392*, 147–154. https://doi.org/10.1016/j.quaint.2015.04.009

19448007, 2026, 20, Downloaded from https://agupubs.onlinelibrary.wiley.com/doi/10.1029/2026GL124581, Wiley Online Library on [18/10/2026]. See the Terms and Conditions (https://onlinelibrary.wiley.com/terms-and-conditions) on Wiley Online Library for rules of use; OA articles are governed by the applicable Creative Commons License